

# One-Dimensional Streamer Simulations Using a Jacobian Free Newton-Krylov Method with Physics Based Preconditioning

Alfredo Duarte\*, Nicholas Deak †, Fabrizio Bisetti‡

The University of Texas at Austin, Austin, Texas, 78712

Numerical simulations of streamers in air at atmospheric pressure and temperature are performed using a one-dimensional finite difference method and implicit time integration. The plasma fluid equations describing a simplified plasma model consisting of electrons, positive ions, and negative ions are made nondimensional and solved with a fully time-implicit and fully coupled approach using variable-order Backward Differentiation Formulas (BDF) and a Jacobian Free Newton-Krylov (JFNK) method. The non-dimensional equations include drift, and diffusive and reactive processes. The kinetics model consists of reactions describing ionization, electron-ion recombination, electron attachment, electron detachment, and ion-ion recombination. A physics based preconditioner is developed that uses operator splitting and linearized operators to address global and local coupling sequentially. The method is applied towards positive streamers in atmospheric air and allows to solve the coupled system of equations in a robust and efficient manner. Numerical tests show that time steps of up to 20 ps are possible with no significant strain on the number of linear and nonlinear iterations, outperforming conventional implicit solvers by orders of magnitude.

#### I. Nomenclature

nondimensional electron number density nnondimensional positive ion number density и nondimensional negative ion number density nondimensional space charge ρ nondimensional electric field nondimensional electric potential associated with space charge nondimensional model constants  $\begin{matrix}c^e_{\rm mxw}\\c^{u,v}_{\rm mxw}\end{matrix}$ nondimensional maxwellian speed of electrons nondimensional maxwellian speed of ions reference degree of ionization  $\tilde{n}_0/\tilde{N}$  $\alpha_0$ nondimensional chemical source term ω  $T_e$ nondimensional electron temperature Tnondimensional gas temperature nondimensional Hopf velocity unit charge (C)  $\tilde{\lambda}_0$ reference Debye length (m) = reference plasma frequency (s<sup>-1</sup>)  $\tilde{\omega}_0$ reference number density (m<sup>-3</sup>)  $\tilde{n}_0$  $\tilde{T}_0$ reference temperature (K) electron and ion mobilities (m<sup>2</sup> V<sup>-1</sup> s<sup>-1</sup>)  $\tilde{\mu}_{e,i}$ vacuum permitivity (F m<sup>-1</sup>)  $\tilde{\epsilon}_0$ background gas temperature (K) background gas number density (m<sup>-3</sup>)  $\tilde{k}_B$ Boltzmann constant (J  $K^{-1}$ ) electron and ion mass (kg)

<sup>\*</sup>Graduate Research Assistant, Department of Aerospace Engineering, The University of Texas at Austin.

<sup>†</sup>Graduate Research Assistant, Department of Aerospace Engineering, The University of Texas at Austin.

<sup>&</sup>lt;sup>‡</sup>Department of Aerospace Engineering, The University of Texas at Austin.

#### **II. Introduction**

The streamer discharge is an important phenomenom for plasmas at atmospheric pressure exposed to high electric fields. The requisite conditions for streamer ignition and propagation can be seen both in nature (lightning), or generated in laboratories with the use of metallic electrodes. When exposed to a high electric field, breakdown of the gas can occur, and an ionization wave is able to propagate through the medium. The propagation of streamers is governed by tightly coupled physical processes that exhibit strong nonlinearities.

Streamers are of practical interest in a number of practical applications, including but not limited to combustion[1–3], ozone generation, and water purification [4]. The production of streamers through Nanosecond Pulsed Discharges (NPD) has emerged as a promising candidate due to higher reduced electric fields when compared to other types of discharges, which leads to higher ionization rates. Reduced electric fields encountered in NPD typically range from 100-1000 Td. The time scales that govern the evolution and propagation of typical streamers [5] (*O* 0.1-100 ns) are usually much lower than, for example, bulk fluid transport time scales (*O* 1-100 ms). The characteristic length scale (Debye length) can be as low as a few micron [6], which is small compared to the lengths of interest, such as those encountered in the glow regime of NPD, which range on the order of *O* 1-10 mm [7]. Due to wide separation between the time and length scales of interest, and those that govern the key processes in discharge dynamics, the development of efficient and stable numerical methods is of central importance.

The numerical simulation of these streamers is a significant challenge and several different numerical methods have been applied in the past. Early discharges relied on the use of explicit methods to solve the governing equations [8, 9], but these are usually restricted to pico-second or sub-picosecond step sizes, which can make simulations of practical applications prohibitively expensive. More recent attempts have developed semi-implicit [10, 11], and even fully implicit [12, 13] methods to relax the time step constraints. However, these implicit schemes do not fully couple the electric potential, instead relying on an explicit prediction.

In this work, the use of a fully-implicit and fully coupled Backward Differentiation Formula (BDF) is applied towards the governing equations. The tight coupling between the species is addressed in the context of the Jacobian Free Newton Krylov (JFNK) method, where an efficient preconditioning strategy is developed to reduce the order of the system. The performance of the solver is then measured through relevant statistics and compared against conventional stiff implicit solvers

# III. Governing Equations and Numerical Model

The plasma model consists of electrons, one class of positive ions and one class of negative ions. Henceforth, dimensional variables are denoted with a tilde, while nondimensional variables are expressed without the tilde. The background gas is atmospheric air at 300 K with number density  $\tilde{N}$  and temperature  $\tilde{T}$ . Both  $\tilde{N}$  and  $\tilde{T}$  are held constant because background air is assumed to evolve on time scales much longer than those associated with streamer propagation (O(1-100) ns). The governing equations are expressed in dimensionless form with the following reference quantities. Lengths are made dimensionless by the Debye length  $\tilde{\lambda}_0 = \sqrt{\tilde{\epsilon}_0 \tilde{k}_B \tilde{T}_0/\tilde{\epsilon}^2 \tilde{n}_0}$  evaluated at reference charge density  $\tilde{n}_0$  and reference temperature  $\tilde{T}_0$ . Here  $\tilde{e}$  is the unit charge,  $\tilde{\epsilon}_0$  the permittivity in vacuum (unity relative permittivity is assumed), and  $\tilde{k}_B$  is Boltzmann's constant. Time is made dimensionless with the plasma period  $2\pi/\tilde{\omega}_0$ , where  $\tilde{\omega}_0 = \sqrt{\tilde{e}^2 \tilde{n}_0/\tilde{\epsilon}_0 \tilde{m}_e}$  is the plasma frequency at reference density  $\tilde{n}_0$ , and  $\tilde{m}_e$  is the electron mass. The electron temperature is normalized by  $\tilde{T}_0$ , chosen to match the electron temperature at the peak electric field value. The dimensionless electric field vector is

$$\theta = -\nabla \varphi + \Omega,\tag{1}$$

where  $\Omega$  is an external potential and  $\varphi$  is the potential associated with space charge, which obeys the Poisson equation

$$-\Delta \varphi = \rho \tag{2}$$

$$\rho = u - v - n. \tag{3}$$

 $\rho$  is the space charge with u, v, and n indicating the number density of cations, anions, and electrons, respectively, as all particles have unit charge. The electric field vector has magnitude  $\theta = |\theta|$ . The non-dimensional conservation equation for the electron number density  $n = n(\mathbf{x}, t)$  is

$$\frac{\partial n}{\partial t} = a_1 \nabla \cdot (\theta n) + a_2 T_e \Delta n + \omega_i - \omega_{er} - \omega_a + \omega_d 
= a_1 (\rho n + \theta \cdot \nabla n) + a_2 T_e \Delta n + \omega_i - \omega_{er} - \omega_a + \omega_d,$$
(4)

where  $\mathbf{x}$  is the position vector, t is time,  $T_e = T_e(\theta)$  is the electron temperature, which is assumed to be a function of  $\theta$  according to the local field approximation and the contribution of  $\nabla T_e$  to the diffusion term is neglected. The terms  $\omega_i$ ,  $\omega_{er}$ ,  $\omega_a$ , and  $\omega_d$  represent sources due to ionization, electron-ion recombination, electron attachment, and electron detachment, respectively. The nondimensional conservation equations for the density of positive ions  $u = u(\mathbf{x}, t)$  and negative ions  $v = v(\mathbf{x}, t)$  are

$$\frac{\partial u}{\partial t} = -a_7(\rho u + \boldsymbol{\theta} \cdot \nabla u) + a_8 \Delta u + \omega_i - \omega_{er} - \omega_{ir}, \tag{5}$$

$$\frac{\partial v}{\partial t} = a_7(\rho v + \boldsymbol{\theta} \cdot \nabla v) + a_8 \Delta v + \omega_a - \omega_{ir} - \omega_d, \tag{6}$$

where  $\omega_{ir}$  represents ion-ion recombination. Expressions for the nondimensional constants  $a_1$ ,  $a_2$ ,  $a_7$ , and  $a_8$  are provided later.

The kinetic model for the three charged particles (electrons, cations, and anions) is adapted from the air plasma kinetic model in Refs. [9, 14]. Ionization is modeled as the ionization of molecular nitrogen  $N_2 + e \longrightarrow e + e + N_2^+$ , electron-ion recombination is modeled as the dissociative recombination  $e + O_2^+ \longrightarrow O + O$ , electron attachment is modeled as the three-body attachment of electrons to molecular oxygen  $e + O_2 + O_2 \longrightarrow O_2^- + O_2$ , electron detachment is modeled by reaction  $O_2^- + O_2 \longrightarrow e + O_2 + O_2$  and ion-ion recombination is modeled as the three-body recombination  $O_2^+ + O_2^- + O_2 \longrightarrow O_2 + O_2 + O_2$ . Based on this reduced kinetic model, the source terms read

$$\omega_i = a_3 \exp(-a_4/\theta)n,\tag{7}$$

$$\omega_{er} = (a_5/T_e)un,\tag{8}$$

$$\omega_a = (a_6/T_e)n,\tag{9}$$

$$\omega_{ir} = a_9 v u, \tag{10}$$

$$\omega_d = r_d v. \tag{11}$$

The expressions for nondimensional constants are defined as

$$a_1 = (2\pi/\tilde{\omega}_0)\tilde{\mu}_e \tilde{N}\tilde{\alpha}_0 \tilde{e}/\tilde{\epsilon}_0, \tag{12}$$

$$a_2 = a_1, \tag{13}$$

$$a_3 = (2\pi/\tilde{\omega}_0)\tilde{c}_s^a \tilde{N},\tag{14}$$

$$a_4 = \tilde{c}_s^b \tilde{\epsilon}_0 / (\tilde{e}\alpha_0 \tilde{\lambda}_0), \tag{15}$$

$$a_5 = (2\pi/\tilde{\omega}_0)\tilde{c}_{18}\tilde{n}_0(300/\tilde{T}_0),\tag{16}$$

$$a_6 = (2\pi/\tilde{\omega}_0)\tilde{c}_{19}\tilde{N}^2(300/\tilde{T}_0),$$
 (17)

$$a_7 = (2\pi/\tilde{\omega}_0)\tilde{\mu}_i \tilde{N}\alpha_0 \tilde{e}/\tilde{\epsilon}_0, \tag{18}$$

$$a_8 = a_7 \tilde{T} / \tilde{T}_0, \tag{19}$$

$$a_9 = (2\pi/\tilde{\omega}_0)\tilde{c}_{22}\tilde{n}_0\tilde{N}. \tag{20}$$

The constants appearing in the parameters for the source terms are taken from select reactions in Refs. [9, 14] and reflect the numbering convention therein:  $\tilde{c}_8^a = 10^{-6} \exp(-8.3 \log 10) = 5.012 \times 10^{-15} \,\mathrm{m}^3 \,\mathrm{s}^{-1}$ ,  $\tilde{c}_8^b = 8.301 \times 10^{-19} \,\mathrm{V} \,\mathrm{m}^2$ ,  $\tilde{c}_{18} = 2 \times 10^{-13} \,\mathrm{m}^3 \,\mathrm{s}^{-1}$ ,  $\tilde{c}_{19} = 8.82 \times 10^{-43} \,\mathrm{m}^6 \,\mathrm{s}^{-1}$ , and  $\tilde{c}_{22} = 2 \times 10^{-37} \,\mathrm{m}^6 \,\mathrm{s}^{-1}$ . The  $r_d$  parameter for electron detachment is modeled as the sum of contributions at low electric fields and high electric fields given by Aleksandrov et. al [15] and Ponomarev et. al. [16], and a function of the electric field. It is of the form

$$r_d = \tilde{k}_d (2\pi/\tilde{\omega}_0) \tilde{N},$$
 
$$\tilde{k}_d = 10^{f(\tilde{T})} + 10^{g(\tilde{\theta}/\tilde{N})}.$$

The expressions for the functional fits of  $f(\tilde{T})$  and  $g(\tilde{\theta}/\tilde{N})$  are provided in the Appendix. Constant normalized mobilities are used, with  $\tilde{\mu}_e \tilde{N} = 10^{24} \text{ V}^{-1} \text{ m}^{-1} \text{ s}^{-1}$  and  $\tilde{\mu}_i \tilde{N} = 6.7 \times 10^{21} \text{ V}^{-1} \text{ m}^{-1} \text{ s}^{-1}$ , which are representative of values that can be calculated from cross sectional data [17, 18].

#### A. Boundary Conditions

Boundary conditions for the electron and ions are Robin boundary conditions from Gorin et. al. [19] and are summarized briefly below.

The boundary conditions for the electron are governed by diffusive losses at both electrodes, as well as secondary emissions at the cathode caused by the flux of positive ions. The dimensionless electron emission flux at the cathode reads

$$\Gamma_{\rm em} = \Gamma_{\rm em}^* + \gamma \Gamma_u, \tag{21}$$

where  $\Gamma_{\rm em}^* \ge 0$  is a prescribed electron flux density emitted from the cathode into the region occupied by the plasma,  $\gamma$  the secondary electron emission coefficient, and  $\Gamma_u$  the flux density of positive ions to the cathode defined as

$$\Gamma_u = \frac{1 - R_u}{1 + R_u} |w^u| u,\tag{22}$$

where  $|w^u|$  is the dimensionless mean speed of the positive ions and  $R_u$  is a reflection coefficient between 0 and 1. The thermal losses are calculated from the thermal velocity given by  $c_{\text{mxw}} = 2\sqrt{8\pi T_e}$ , which has a dependence on the electron temperature  $T_e$ , and thus the electric field magnitude  $\theta$ .

The boundary conditions for the ions are more complicated, and may change depending on the strength of the reduced electric field. Under the assumption of a *weak field*, the ion boundary conditions take on a form similar to that of the electrons, with a thermal velocity calculated using the gas temperature T. Alternatively, under the assumption of a large electric field, the *strong field* approximation is more suitable, in which case the ion boundary conditions are dominated by drift processes,

$$|w^{u,v}| = \begin{cases} c_{\text{mxw}}^{u,v}/2, & \text{weak field} \\ a_7|\theta|, & \text{strong field} \end{cases}$$
 (23)

In the above  $c_{\text{mxw}}^{u,v}$  is the Maxwellian speed for the ions evaluated at the background gas temperature  $c_{\text{mxw}}^{u,v} = 2\sqrt{8\pi T m_e/m_i}$ . In this work, the applied electric field component is large enough that a strong field approximation for the ions at the boundaries is appropriate. Overall, these effects are captured by the Robin boundary condition for a charged particle  $\phi$ 

$$-D\frac{\partial \phi}{\partial \hat{x}} + V\phi = \chi, \tag{24}$$

where D is the diffusion coefficient, V is the Hopf velocity describing thermal and drift effects,  $\hat{x}$  is the local coordinate pointing away from the plasma and into the electrode, and  $\chi$  are secondary particle emissions at the electrode.

# B. One-dimensional plasmas between electrodes with applied voltage

We seek to simulate the temporal evolution of the density of all charges in between two parabolic and axisymmetric pin electrodes subject to a voltage pulse consistent with a nanosecond pulsed discharge. To this end, we assemble a one-dimensional computational model, letting  $x \in [0, H]$  be the coordinate along the axis connecting the tips of the two electrodes across the gap. The anode is at x = 0 and the cathode is at x = H. A schematic is shown in Fig.1 (b).

The transport equations for the charges are evaluated at the centerline r=0 and the contribution of charge diffusion in the radial direction is neglected, e.g. it is assumed that  $\partial^2 n/\partial r^2 = 0$  and similarly for u and v. Further, all radial derivatives at the axis vanish due to symmetry about the axis.

The electric field on the axis is assumed to be equal to the sum of two contributions, yielding the so-called "1.5-dimensional model" of pin-to-pin discharges:

$$\theta(x,t) = \theta_0 + \Theta,\tag{25}$$

where  $\Theta(x,t)$  is the electric field associated with the potential due to a prescribed, unsteady bias voltage and  $\theta_{\rho}(x,t)$  that due to the space charge.

The first contribution  $\Theta(x,t)$  consists of the axial component of the electric field due to a bias voltage applied to the axisymmetric pin electrodes. This component is calculated by solving a Poisson equation in an axisymmetric domain for a unit voltage bias. The solution is shown in Fig. 1(a). The electric field component is then rescaled as needed to reflect the actual voltage bias at a given time.

The second contribution is due to the space charge and is calculated as proposed by [20]. Briefly, at each axial location along the gap, the charges are assumed to be distributed uniformly radially in the range  $0 \le r \le R$  and zero for

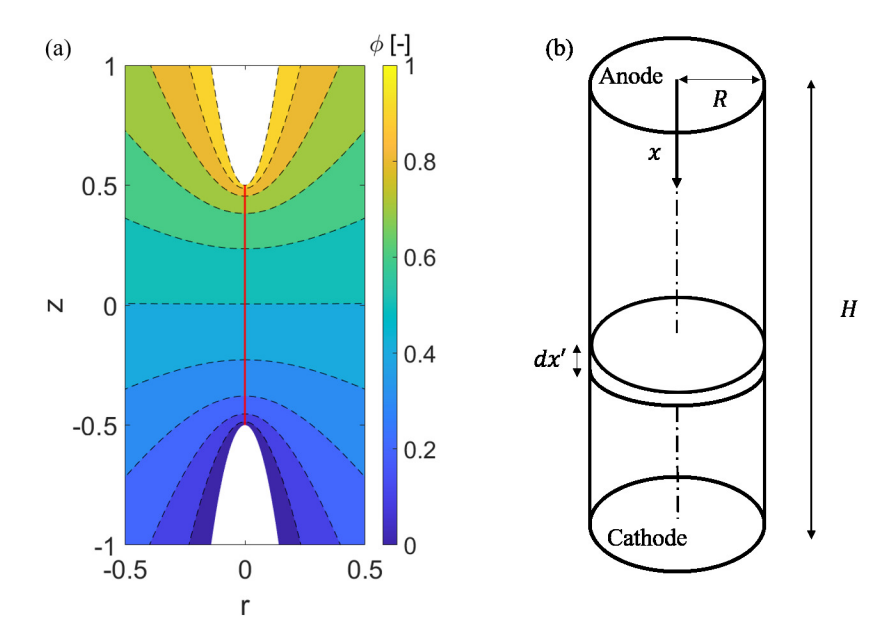


Fig. 1 (a) Potential axisymmetric solution of parabolic pins with radius of curvature 400  $\mu m$  and gap length 1 cm with centerline in red, along with (b) the schematic of the simplified 1-D configuration.

r > R. The charge density at each axial location is taken to be equal to the solution from the one-dimensional restriction of the charge conservation equations on the axis. In other words, the charges are modeled as if they are arranged in a cylinder of prescribed radius R and height H, homogeneously radially, but inhomogeneously axially. Further, it is assumed that the top and bottom cylinder surfaces are capped by infinite grounded planes oriented such that their normal is parallel to the axis. A schematic of the charge arrangement is shown in Fig. 1(b).

The potential associated with such a charge distribution and grounded infinite planes at x = 0 and H is solved for by superposition and method of images as discussed in [20]. Once the potential is available, its gradient is evaluated on the axis, providing the electric field component associated with the space charge

$$\theta_{\rho}(x) = \int_{-x}^{H-x} -\rho_{\varphi}(x+x') \left(\frac{x'}{2\sqrt{R^2 + x'^2}}\right) dx'. \tag{26}$$

Image charges extending a length of H from the left and right boundaries of the domain are included to satisfy the induced potential at the boundaries. In this work, we set H/R = 20, i.e. we assume that the charges are arranged in a cylinder with radius equal to  $0.05H \ll H$ .

The boundary conditions in one dimension are summarized in Tab. 1.

Table 1 Robin boundary conditions for electrons, positive ions, and negative ions.

Particle	Electrode	<b>Boundary Condition</b>	Hopf velocity V
electron	anode	$-a_2 T_e \partial n / \partial x + V n = 0$	$g_1(R_n)c_{\text{mxw}}/2 - a_1\theta$
electron	cathode	$a_2 T_e \partial n / \partial x + V n = g_2(R) \Gamma_{\text{em}}$	$g_1(R_n)c_{\text{mxw}}/2 + a_1\theta$
positive ion	anode	$-a_8\partial u/\partial x + Vu = 0$	$g_1(R_u) w^u +a_7\theta$
positive ion	cathode	$a_8\partial u/\partial x + Vu = 0$	$g_1(R_u) w^u -a_7\theta$
negative ion	anode	$-a_8\partial v/\partial x + Vv = 0$	$g_1(R_v) w^v -a_7\theta$
negative ion	cathode	$a_8\partial v/\partial x + Vv = 0$	$g_1(R_v) w^v +a_7\theta$

The functions  $g_1$  and  $g_2$  are defined as  $g_1(x) = (1-x)/(1+x)$  and  $g_2(x) = 2/(1+x)$ , respectively.  $R_n$ ,  $R_u$ , and  $R_v$  are the reflection coefficients of each particle, in this study assumed to be 0 for all charged species. The nondimensional Hopf velocity defined in Tab. 1 accounts for the effect of thermal velocity, drift velocity, and reflection.

#### C. Fully Coupled Implicit Time Discretization

Consider a Backward Differentiation Formula (BDF) of order s from time  $t_n$  to  $t_{n+1} = t_n + h$ 

$$\left(\alpha y^{n+1} + \sum_{k=0}^{s-1} \beta_k y^{n-k}\right) = f(t^{n+1}, y^{n+1}). \tag{27}$$

In general, the BDF coefficients  $\alpha$  and  $\beta_k$  depend on order s, current time step, and time step history. The residual functions for the nonlinear system of equations are obtained by applying the time discretization to equations (4)-(6)

$$F_n(\mathbf{n}, \mathbf{u}, \mathbf{v}, \mathbf{\phi}) = \left(\alpha \mathbf{n} + \sum_{k=0}^{s-1} \beta_k n^{n-k}\right) - a_2 T_e(L\mathbf{n}) - a_1 (\theta D_-) \mathbf{n} - a_1 \rho \mathbf{n},$$

$$- r_3 \mathbf{n} + r_5 \mathbf{u} \mathbf{n} + r_6 \mathbf{n} - r_d \mathbf{v}$$
(28)

$$F_{u}(\mathbf{n}, \mathbf{u}, \mathbf{v}, \mathbf{\phi}) = \left(\alpha \mathbf{u} + \sum_{k=0}^{s-1} \beta_{k} u^{n-k}\right) - a_{8} L \mathbf{u} + a_{7} (\theta D_{+}) \mathbf{u} + a_{7} \rho \mathbf{u}$$

$$- r_{3} \mathbf{n} + r_{5} \mathbf{u} \mathbf{n} + a_{9} \mathbf{v} \mathbf{u}, \tag{29}$$

$$F_{\nu}(\mathbf{n}, \mathbf{u}, \mathbf{v}, \mathbf{\phi}) = \left(\alpha \mathbf{v} + \sum_{k=0}^{s-1} \beta_k \nu^{n-k} \right) - a_8 L \mathbf{v} - a_7 (\theta D_-) \mathbf{v} - a_7 \rho \mathbf{v}$$
$$- r_6 \mathbf{n} + a_9 \mathbf{v} \mathbf{u} + r_d \mathbf{v}, \tag{30}$$

$$F_{\omega}(\mathbf{n}, \mathbf{u}, \mathbf{v}, \boldsymbol{\varphi}) = -L_{R}\boldsymbol{\varphi} - (\mathbf{u} - \mathbf{v} - \mathbf{n}), \tag{31}$$

where n, u, v, and  $\varphi$  are the unknowns at time  $t_{n+1}$ , i.e. number densities and potential induced by the space charge.

$$\rho_{\varphi} = \mathbf{u} - \mathbf{v} - \mathbf{n},\tag{32}$$

$$T_{e} = T_{e}(\theta), \tag{33}$$

$$r_3 = r_3(\theta) = a_4 \exp(-a_4/|\theta|),$$
 (34)

$$r_5 = r_5(T_e) = a_5/T_e,$$
 (35)

$$r_6 = r_6(T_e) = a_6/T_e, (36)$$

$$r_d = r_d(\theta). \tag{37}$$

The electric field is evaluated at  $t_{n+1}$  as required by a fully implicit approach

$$\theta = \theta(t_{n+1}, \varphi) = -D\varphi + \Theta(t_{n+1}), \tag{38}$$

with  $\varphi$  satisfying the discrete form of the Poisson equation

$$-L_R \varphi = \rho_{\varphi}. \tag{39}$$

 $\rho = \rho_{\varphi} + \partial \Theta(t)/\partial x$  is equal to the sum of the space charge and the gradient of external electric field  $\Theta(t)$  to simplify expressions. The discrete operator  $\theta D_{\pm}$  is a suitable finite difference approximation to  $\theta \partial/\partial x$  upwinded using the Quadratic Upstream Interpolation for Convective Kinematics (QUICK) [21] scheme for the respective particle depending on the sign of  $\theta$  at time step n+1 as required by the implicit nature of the temporal discretization. Further, D and D are centered, second-order finite differences approximations to  $D/\partial x$  and  $D/\partial x^2$ . Finally,  $D/\partial x$  represents the discrete form of Eq.(26) using a  $D/\partial x$  order trapezoidal quadrature for the integration.

The boundary conditions provide 6 additional algebraic constraints and 6 additional residual functions are defined

$$F_n^0(\mathbf{n}, \mathbf{v}, \mathbf{u}, \mathbf{\phi}) = -a_2 T_e D_0 \mathbf{n} + V_{n,0} \mathbf{n}_0, \tag{40}$$

$$F_n^H(n, v, u, \varphi) = a_2 T_e D_H n + V_{n,H} n_H - g_2(R) \Gamma_{em},$$
 (41)

$$F_u^0(\mathbf{n}, \mathbf{v}, \mathbf{u}, \mathbf{\phi}) = -a_8 D_0 \mathbf{u} + V_{u,0} \mathbf{u}_0, \tag{42}$$

$$F_u^H(n, v, u, \varphi) = a_8 D_H u + V_{u,H} u_H, \tag{43}$$

$$F_{\nu}^{0}(\mathbf{n}, \mathbf{v}, \mathbf{u}, \mathbf{\phi}) = -a_{8}D_{0}\mathbf{v} + V_{\nu,0}\mathbf{v}_{0}, \tag{44}$$

$$F_{\nu}^{H}(\mathbf{n}, \mathbf{v}, \mathbf{u}, \mathbf{\phi}) = a_{8}D_{H}\mathbf{v} + V_{\nu, H}\mathbf{v}_{H}, \tag{45}$$

where  $D_0$  and  $D_H$  are discrete, one-sided  $2^{\text{nd}}$  order accurate finite difference operators at  $\tilde{x} = 0$  and  $\tilde{x} = H$ , respectively. It is apparent that the electron temperature, Hopf velocities, and electron emission flux density all depend on the unknowns.

#### D. Physics Based Preconditioning

The system of equations derived in the previous section is solved with a Jacobian-free Newton Krylov (JFNK) method [22]. The JFNK is a nested iterative method consisting of two levels: one outer loop over the Newton corrections, and one inner loop to build the Krylov subspace for each Newton correction required. Each Newton iteration solves the system

$$J\delta x = -F(x),\tag{46}$$

where J is the Jacobian matrix,  $\delta x$  the Newton update, and F(x) is the residual of the nonlinear function. The Jacobian matrix itself is not needed, and the only input required is the calculation of Jacobian-matrix-vector products approximated by finite difference

$$Jv = \frac{F(x + \epsilon v) - F(x)}{\epsilon},\tag{47}$$

where v is a vector and  $\epsilon$  a small perturbation. Within the Krylov loop, a preconditioner is usually required to reduce the number of Krylov iterations by clustering eigenvalues efficiently. An appropriate preconditioner is needed to accelerate the convergence of the Generalized Minimal Residual Method (GMRES) in the context of the JFNK solver. A successful preconditioner matrix P approximates the Jacobian of the residual function as closely as possible, solving the system

$$JP^{-1}P\delta x = -F(x). \tag{48}$$

The preconditioning strategy presented below is based on the work of Mosseau et. al. [23], where equations are linearized, and operator splitting is used to approximate the Jacobian with products of matrices that can be factorized easily. The first step consists of linearizing the fully implicit system of equations.  $\theta^{n+1}$  is approximated as

$$\boldsymbol{\theta}^{n+1} \approx \boldsymbol{\theta}^{\bullet} = \theta(t_{n+1}, \varphi) = -D\varphi + \Theta(t_{n+1}), \tag{49}$$

whereby the space charge contribution is extrapolated from  $t_n$  to  $t_{n+1}$  with the same order of accuracy as the BDF formula, while the external electric field is evaluated at  $t_{n+1}$  directly. Then, the drift operator becomes

$$\theta^{n+1}D_+ \approx \theta^{\bullet}D_+,\tag{50}$$

where upwinding of the discrete first derivative  $D_{\pm}$  is based on the local value of the electric field  $\theta^{\bullet}$ , as well as the sign of the particle charge. Similarly,  $T_e^{n+1}$  in the diffusive term for the electrons is approximated by evaluating the electron temperature at  $|\theta^{\bullet}|$ 

$$T_e^{n+1} \approx T_e^{\bullet} = T_e(|\theta^{\bullet}|) \tag{51}$$

and the four rate constants read

$$r_3^{n+1} \approx r_3^{\bullet} = r_3(\theta^{\bullet}) = a_4 \exp(-a_4/|\theta^{\bullet}|),$$
 (52)

$$r_5^{n+1} \approx r_5^{\bullet} = r_5(T_{\rho}^{\bullet}) = a_5/T_{\rho}^{\bullet}, \tag{53}$$

$$r_6^{n+1} \approx r_6^{\bullet} = r_6(T_e^{\bullet}) = a_6/T_e^{\bullet},$$
 (54)

$$r_d^{n+1} \approx r_d^{\bullet} = r_d(\theta^{\bullet}),\tag{55}$$

(56)

Products of the form  $a^{n+1}b^{n+1}$  are linearized as

$$a^{n+1}b^{n+1} = (a^n + \delta a)(b^n + \delta b) = a^n b^n + a^n \delta b + b^n \delta a.$$
 (57)

The increments of the solution vector components are defined as

$$\delta n = n^{n+1} - n^n \tag{58}$$

$$\delta u = u^{n+1} - u^n \tag{59}$$

$$\delta v = v^{n+1} - v^n \tag{60}$$

$$\delta\varphi = \varphi^{n+1} - \varphi^n \tag{61}$$

and  $\delta \rho = \delta u - \delta v - \delta n$ .

The linear system in equations (28)-(30) is of order 3m, where m is the number of discrete spatial locations. Thus, operator splitting is used to lower the order of the system. Intermediate field increments are introduced, which are solved for independently, and then coupling among fields at each spatial grid point is enforced. This results in a linear system for the intermediate increment  $\delta n^*$ 

$$[\alpha - (a_2 T_e^{\bullet} L + a_1 \theta^{\bullet} D_- + a_1 \rho^n - a_1 n^n + r_3^{\bullet} - r_5^{\bullet} u^n - r_6^{\bullet})] \delta n^*$$
  
=  $-F_n(n^n, u^n, v^n, \varphi^n).$  (62)

Similarly, for the positive and negative ions' intermediate increments  $\delta u^*$  and  $\delta v^*$ , solve

$$[\alpha - (a_8 L - a_7 \theta^{\bullet} D_+ - a_7 \rho^n - a_7 u^n - r_5^{\bullet} n^n - a_9 v^n)] \delta u^*$$
  
=  $-F_u(n^n, u^n, v^n, \varphi^n),$  (63)

and

$$[\alpha - (a_8 L + a_7 \theta^{\bullet} D_- + a_7 \rho^n - a_7 v^n - a_9 u^n - r_d^{\bullet})] \delta v^*$$
  
=  $-F_v(n^n, u^n, v^n, \varphi^n).$  (64)

The three linear systems above are of order m and are solved independently for  $\delta n^*$ ,  $\delta u^*$ , and  $\delta v^*$ . Once the three intermediate increments are available, m independent  $3 \times 3$  linear systems are solved, each consisting of three coupled linear equations

$$\alpha \delta n + (r_5^{\bullet} n^n - a_1 n^n) \delta u + (a_1 n^n - r_d^{\bullet}) \delta v = \alpha \delta n^*, \tag{65}$$

$$(r_5^{\bullet}u^n - a_7u^n - r_3^{\bullet})\delta n + \alpha \delta u + (a_9u^n - a_7u^n)\delta v = \alpha \delta u^*, \tag{66}$$

$$(a_7 v^n - r_6^{\bullet}) \delta n + (-a_7 v^n - a_9 v^n) \delta u + \alpha \delta v = \alpha \delta v^*. \tag{67}$$

It is noted that other than the terms originating from drift and diffusion (terms with  $a_1$ ,  $a_2$ ,  $a_7$ , or  $a_8$ ), the components of the systems of equations above are from the Jacobian of the kinetic terms and may be generalized to arbitrary kinetics easily. The third and final step consists in solving for the increment of the potential  $\delta\varphi$ 

$$-L_R\delta\varphi = \delta u - \delta v - \delta n,\tag{68}$$

which is also a linear system of order m and the linear operator remains unchanged with respect to the original system. Similarly, the same approximations and linearizations are applied at the boundaries and incorporated into the preconditioning framework. In incremental form, the updates for  $\delta n_{0,H}$ ,  $\delta u_{0,H}$ , and  $\delta v_{0,H}$  read

$$-a_2 T_{\rho}^{\bullet} D_0 \delta n + V^{\bullet} \delta n_0 = -F_{\rho}^0 (n^n, v^n, u^n, \varphi^n), \tag{69}$$

$$a_2 T_{\rho}^{\bullet} D_H \delta n + V^{\bullet} \delta n_H = -F_n^H (n^n, v^n, u^n, \varphi^n), \tag{70}$$

$$-a_8 D_0 \delta u + V^{\bullet} \delta u_0 = -F_u^0(n^n, v^n, u^n, \varphi^n), \tag{71}$$

$$a_8 D_H \delta u + V^{\bullet} \delta u_H = -F_u^H (n^n, v^n, u^n, \varphi^n), \tag{72}$$

$$-a_8 D_0 \delta v + V^{\bullet} \delta v_0 = -F_0^0(n^n, v^n, u^n, \varphi^n), \tag{73}$$

$$a_8 D_H \delta v + V^{\bullet} \delta v_H = -F_v^H (n^n, v^n, u^n, \varphi^n). \tag{74}$$

The equations above are added to each of the 3 independent linear systems for n, u, and v in Eq. (62), (63), and (64). The second step of the preconditioner strategy consists in solving coupling among charged particles. Because the approximations introduced removed the coupling, the second step is not necessary at the boundaries.

## **IV. Results**

The model presented is used to solve streamer discharges in air across a gap of H=1 cm with a radius R=0.5 mm. The applied electric field  $\Theta(t,x)$  is the axial component of the electric field associated with the potential in between two axisymmetric parabolic pins as shown in Fig. (1). The pins have a radius of curvature equal to  $400~\mu m$ . The spatial profile is calculated once for a unit voltage bias and then multiplied by a factor  $\sigma(t)$ , which is modeled as a Gaussian with a specified peak and full width half max (FWHM). Operators with  $2^{nd}$  order spatial accuracy are used, and a  $2^{nd}$  order fixed leading coefficient BDF formula is used to recycle matrix factorizations as much as possible. The solution is started from a steady solution with no applied electric field and a background ionization of  $10^7~m^{-3}s^{-1}$  [24]. Lower-upper (LU) decomposition is used to factorize the preconditioner matrices, and the stopping criteria from SUNDIALS' CVODE is borrowed for both the linear and nonlinear iterations [25]. The chosen reference values are  $\tilde{n}_0 = 10^{18}~m^{-3}$  and  $\tilde{T}_0 = 4.118 \times 10^4~K$ , and all other reference values are then calculated. The number densities of electrons, positive ions, negative ions, and the resulting reduced electric field are shown in Fig. 2 for a gap discharge with a pulse peak of 50 kV and a 50 ns FWHM (peak at 100 ns) with the coarsest mesh that allowed for a physical solution to be obtained (1250 grid points, a resolution of 10  $\mu$ m in the middle, and refined near the boundaries to 0.1  $\mu$ m with a constant stretch rate).

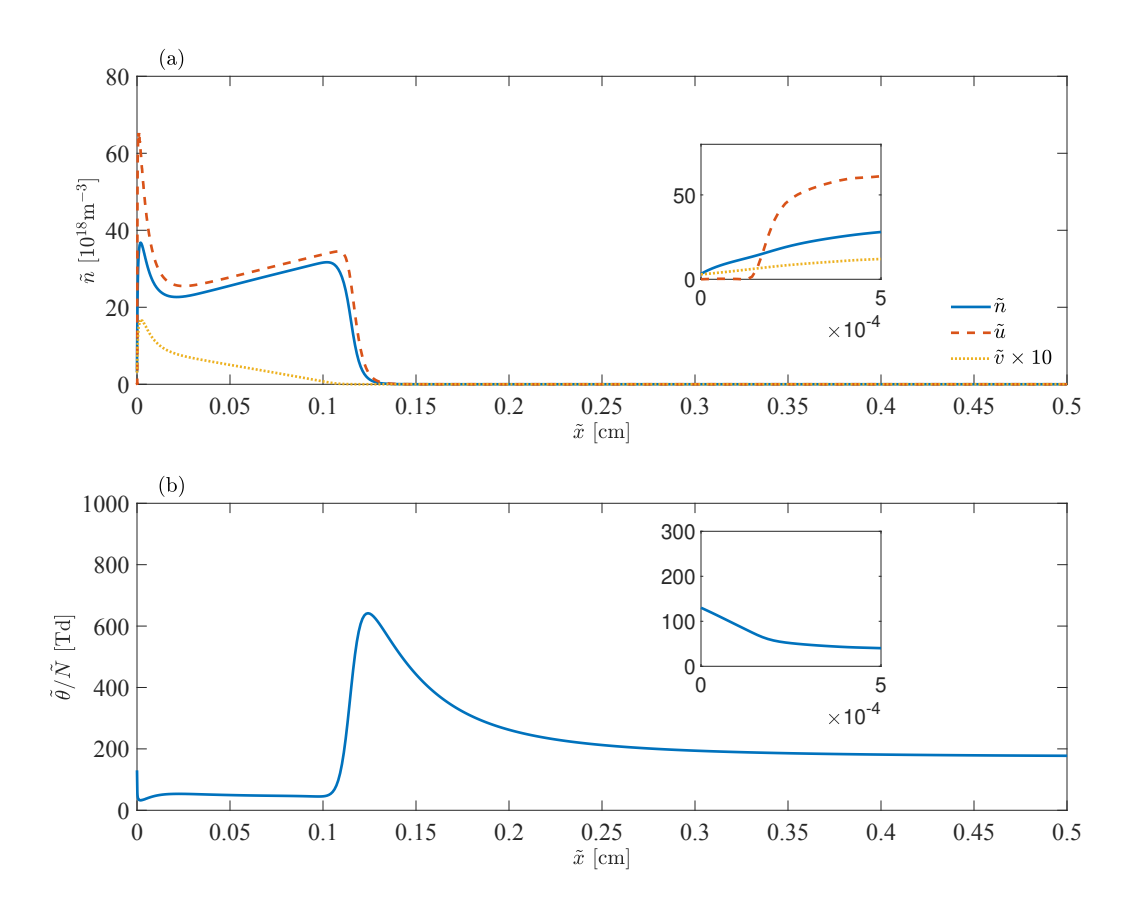


Fig. 2 (a) Number densities  $\tilde{n}$ ,  $\tilde{u}$ ,  $\tilde{v}$ , and (b) reduced electric field  $\tilde{\theta}/\tilde{N}$  of a positive streamer discharge in air; both at  $\tilde{t} = 102.3$  ns

Features that are characteristic of nanosecond pulse filamentary discharges become apparent. In Fig. 2 (a), an accumulation of positive charge on the anode developed into a streamer that propagates through the gap. In Fig. 2 (b), the reduced electric field across the gap exhibits significant shielding at the anode (x = 0) and a strong induced electric field at the streamer head. Insets on Fig. 2 show the thin boundary layer where charge separation is observed, which causes the slight uptick in the electric field near the anode.

Two of the most significant statistics for a JFNK solver are the number of linear and nonlinear iterations required to

compute the solution. These two quantities provide costs that are more or less independent from the computing machine, matrix factorization, and grid size. Fig. 3 (a) shows the time step history compared to the chemical, advective, and dielectric time scales for the coarsest grid. The advective time scale is calculated using the maximum drift velocity, while the chemical time scale corresponds to  $1/|\lambda_c|$ , where  $|\lambda_c|$  is the largest eigenvalue as computed based on the kinetics Jacobian at every grid point. Fig. 3 (b) shows the number of linear and nonlinear iterations used to compute the solution. The temporal variation of the time step sizes is such that the time step is always smaller than the dielectric relaxation time. Exceeding the dielectric time scale results in large inaccuracies that lead to an unstable solution even when using the second order BDF. After the discharge begins around 98 ns, the preconditioning strategy allows time steps of the order of around 20 ps consistently. The number of nonlinear iterations never exceeds 3 and the average number of linear iterations per nonlinear iteration does not exceed 7.

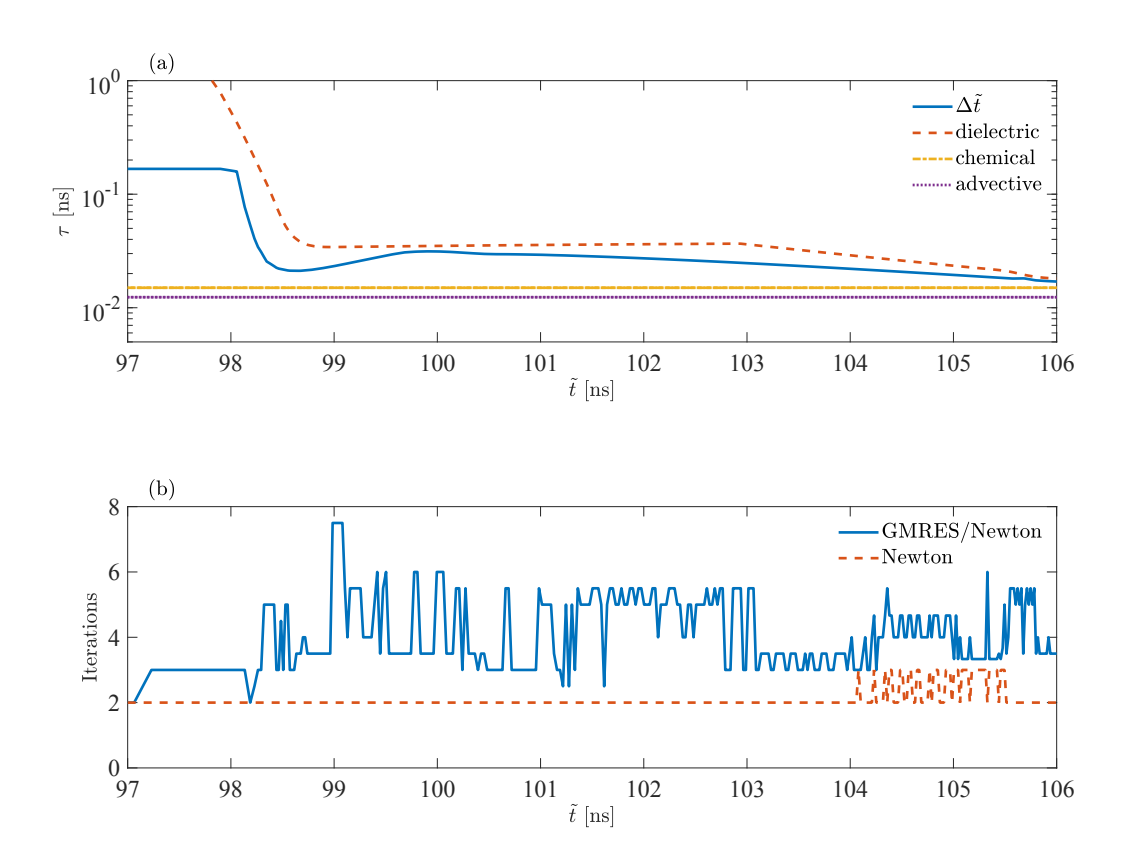


Fig. 3 (a) Time step history along with limiting time scales and (b) iteration statistics for the simulation shown in Fig. 2

Fig. 4 provides a summary of the time taken to simulate the entire discharge from a steady state solution until the streamer closed 9 tenths of the gap. Three different grid sizes where used, ranging from 1250 grid points up to 5000 grid points. The f factor shown represents the number of preconditioners computed per time step; for example, a factor of f = 0.5 indicates that the same preconditioner matrix factors are used 2 consecutive time steps, reducing the computational costs significantly. The use of the coarsest mesh allows to complete one simulation in less than 5 minutes. For comparison, solving the system of equations with the stiff implicit MATLAB solver ode15s with the coarsest mesh (1250 grid points, a resolution of 10  $\mu$ m in the middle, and refined near the boundaries to 0.1  $\mu$ m with a constant stretch rate) and a dense finite difference Jacobian required 4 hours.

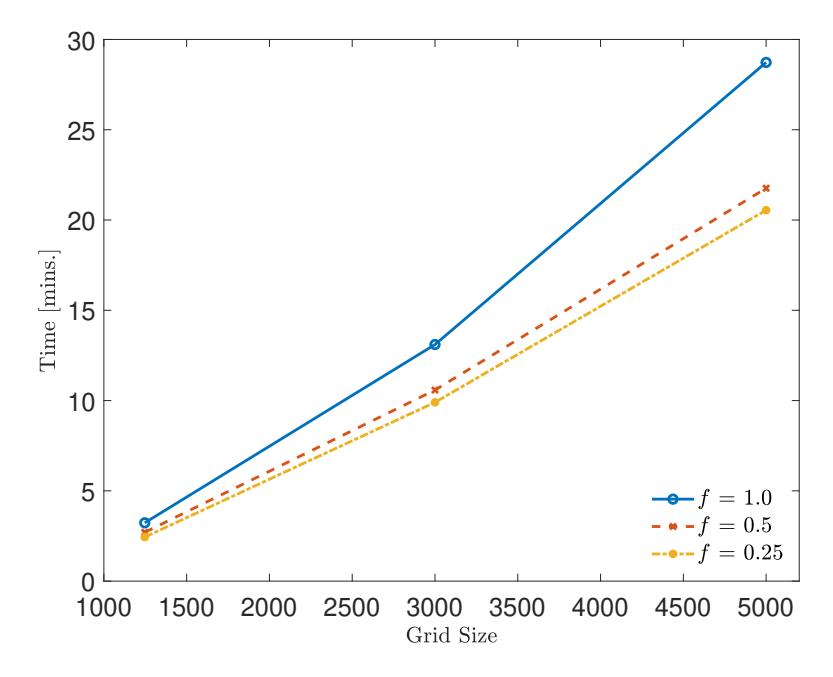


Fig. 4 Performance times for different grids reusing matrix factorizations with the same simulation parameters as those described for Fig. 2

#### V. Conclusions

A system of equations with the drift-diffusion model and simplified kinetics is formulated for the simulation of pin to pin plasma discharges in atmospheric air at 300 K. Once discretized in time, the resulting system of equations is fully implicit and couples electrons, positive ions, and negative ions. A physics based preconditioning framework is developed by splitting global coupling for each individual particle and local coupling between charges. The physics based preconditioner is then applied with a Jacobian Free Newton-Krylov method using 2<sup>nd</sup> order spatial operators and a 2<sup>nd</sup> order BDF formula in time. Results show the ability to simulate gap discharges with time steps around 20 ps. These time steps exceed advective and chemical time scales, and are mainly limited by accuracy. We find that the largest accurate time step possible is approximately equal to the dielectric relaxation time. The number of linear and nonlinear iterations remains low throughout the simulation, and times-to-solution are orders of magnitude shorter than with dense finite difference Jacobian approximations used by common stiff solvers such as MATLAB ode15s or SUNDIALS' CVODE [25].

# A. Appendix

## A. Detachment functional fits

The dimensional detachment rate constant is given by

$$\tilde{k}_d = 10^{f(\tilde{T})} + 10^{g(\tilde{\theta}/\tilde{N})} \text{ [cm}^3/\text{s]},$$

where the temperature dependent component  $f(\tilde{T})$  is a second order polynomial and the component that depends on the reduced electric field  $f(\tilde{\theta}/\tilde{N})$ , is a fourth order polynomial. The exact expressions of the fits are,

$$\begin{split} f(\tilde{T}) &= c_{d1}\tilde{T}^2 + c_{d2}\tilde{T} + c_{d3}, \\ g(\tilde{\theta}/\tilde{N}) &= c_{d4}(\tilde{\theta}/\tilde{N})^4 + c_{d5}(\tilde{\theta}/\tilde{N})^3 + c_{d6}(\tilde{\theta}/\tilde{N})^2 + c_{d7}(\tilde{\theta}/\tilde{N}) + c_{d8}, \\ c_{d1} &= -2.026 \text{x} 10^{-5}, \\ c_{d2} &= 3.062 \text{x} 10^{-2}, \\ c_{d3} &= -2.470 \text{x} 10^1, \\ c_{d4} &= -1.319 \text{x} 10^{-9}, \\ c_{d5} &= 1.305 \text{x} 10^{-6}, \\ c_{d6} &= -4.818 \text{x} 10^{-4}, \\ c_{d7} &= 8.344 \text{x} 10^{-2}, \\ c_{d8} &= -1.653 \text{x} 10^1. \end{split}$$

The polynomials were fit to the data reported in Fig. 2 in [15] and Fig. 11 in [16].

#### References

- [1] Ju, Y., and Sun, W., "Plasma assisted combustion: Dynamics and chemistry," *Prog. Energy and Combust. Sci.*, Vol. 48, 2015, pp. 21–83.
- [2] Starikovskii, A. Y., Nikipelov, A., Nudnova, M., and Roupassov, D., "SDBD plasma actuator with nanosecond pulse-periodic discharge," *Plasma Sources Sci. Technol.*, Vol. 18, No. 3, 2009, p. 034015.
- [3] Deak, N., Bellemans, A., and Bisetti, F., "Plasma-assisted ignition of methane/air and ethylene/air mixtures: Efficiency at low and high pressures," *Proc. Combust. Inst.*, 2020.
- [4] Akiyama, H., "Streamer discharges in liquids and their applications," *IEEE Trans. Dielectr. Electr. Insul.*, Vol. 7, No. 5, 2000, pp. 646–653.
- [5] Vitello, P., Penetrante, B., and Bardsley, J., "Simulation of negative-streamer dynamics in nitrogen," *Phys. Rev. E*, Vol. 49, No. 6, 1994, p. 5574.
- [6] Unfer, T., Boeuf, J.-P., Rogier, F., and Thivet, F., "An asynchronous scheme with local time stepping for multi-scale transport problems: Application to gas discharges," J. Comput. Phys., Vol. 227, No. 2, 2007, pp. 898–918.
- [7] Pai, D. Z., Stancu, G. D., Lacoste, D. A., and Laux, C. O., "Nanosecond repetitively pulsed discharges in air at atmospheric pressure—the spark regime," *Plasma Sources Sci. Technol.*, Vol. 18, No. 4, 2009, p. 045030.
- [8] Kulikovsky, A., "Two-dimensional simulation of the positive streamer in N2 between parallel-plate electrodes," J. Phys. D Appl. Phys., Vol. 28, No. 12, 1995, p. 2483.
- [9] Pancheshnyi, S. V., and Starikovskii, A. Y., "Two-dimensional numerical modelling of the cathode-directed streamer development in a long gap at high voltage," *J. Phys. D: Appl. Phys.*, Vol. 36, 2003, pp. 2683–2691.
- [10] Teunissen, J., and Ebert, U., "Afivo: A framework for quadtree/octree AMR with shared-memory parallelization and geometric multigrid methods," Comput. Phys. Commun., Vol. 233, 2018, pp. 156–166.
- [11] Marskar, R., "An adaptive Cartesian embedded boundary approach for fluid simulations of two-and three-dimensional low temperature plasma filaments in complex geometries," J. Comput. Phys., Vol. 388, 2019, pp. 624–654.
- [12] Van Dijk, J., Peerenboom, K., Jimenez, M., Mihailova, D., and Van der Mullen, J., "The plasma modelling toolkit Plasimo," *J. Phys. D Appl. Phys.*, Vol. 42, No. 19, 2009, p. 194012.
- [13] Breden, D., Raja, L. L., Idicheria, C. A., Najt, P. M., and Mahadevan, S., "A numerical study of high-pressure non-equilibrium streamers for combustion ignition application," J. Appl. Phys., Vol. 114, No. 8, 2013, p. 083302.
- [14] Kossyi, I. A., Kostinsky, A. Y., Matveyev, A. A., and Silakov, V. P., "Kinetic scheme of the non-equilibrium discharge in nitrogen-oxygen mixtures," *Plasma Sources Sci. Technol.*, Vol. 1, 1992, p. 207.
- [15] Aleksandrov, N. L., and Anokhin, E. M., "Electron detachment from O2 ions in oxygen: the effect of vibrational excitation and the effect of electric field," J. Phys. B, Vol. 44, No. 11, 2011, p. 115202.
- [16] Ponomarev, A. A., and Aleksandrov, N. L., "Monte Carlo simulation of electron detachment properties for O2- ions in oxygen and oxygen:nitrogen mixtures," *Plasma Sources Sci. Technol.*, Vol. 24, No. 3, 2015, p. 035001.
- [17] Hagelaar, G., and Pitchford, L., "Solving the Boltzmann equation to obtain electron transport coefficients and rate coefficients for fluid models," *Plasma Sources Sci. Technol.*, Vol. 14, No. 4, 2005, p. 722.
- [18] Bisetti, F., and El Morsli, M., "Calculation and analysis of the mobility and diffusion coefficient of thermal electrons in methane/air premixed flames," Combust. Flame, Vol. 159, No. 12, 2012, pp. 3518–3521.
- [19] Gorin, V., Kudryavtsev, A., Yao, J., Yuan, C., and Zhou, Z., "Boundary conditions for drift-diffusion equations in gas-discharge plasmas," *Phys. Plasmas*, Vol. 27, No. 1, 2020, p. 013505.
- [20] Davies, A., Evans, C., and Jones, F. L., "Electrical breakdown of gases: the spatio-temporal growth of ionization in fields distorted by space charge," *Proc. R. Soc. Lond. Series A. Mathematical and Physical Sciences*, Vol. 281, No. 1385, 1964, pp. 164–183.
- [21] Leonard, B., "A stable and accurate convective modelling procedure based on quadratic upstream interpolation," Comput Methods Appl. Mech. Eng, Vol. 19, No. 1, 1979, pp. 59–98.

- [22] Knoll, D., and Keyes, D., "Jacobian-free Newton–Krylov methods: a survey of approaches and applications," *J. Comput. Phys.*, Vol. 193, No. 2, 2004, pp. 357–397.
- [23] Mousseau, V., Knoll, D., and Rider, W., "Physics-Based Preconditioning and the Newton–Krylov Method for Non-equilibrium Radiation Diffusion," *J. Comput. Phys.*, Vol. 160, No. 2, 2000, pp. 743–765.
- [24] Deak, N. E., Duarte, A., and Bisetti, F., "Steady-State Streamer Simulations Using a Spectral Deferred Correction Strategy," AIAA Scitech 2021 Forum, 2021.
- [25] Hindmarsh, A. C., Brown, P. N., Grant, K. E., Lee, S. L., Serban, R., Shumaker, D. E., and Woodward, C. S., "SUNDIALS: Suite of nonlinear and differential/algebraic equation solvers," *ACM Trans. Math. Software*, Vol. 31, No. 3, 2005, pp. 363–396.